Kinetic study of reaction formation of phosphate products from thermal dissolution of wolframite using fusion technique

by T.T. Chiweshe[1], L.S. Mokhahlane[2], and M. Welman-Purchase[3]

Affiliation:
[1]University of Free State, Institute for Groundwater Studies, Bloemfontein, South Africa
[2]University of the Witwatersrand, Johannesburg, South Africa
[3]University of Free State, Geology Department, Bloemfontein, South Africa

Correspondence to:
L.S. Mokhahlane

Email:
sehai.mokhahlane@wits.ac.za

Dates:
Received: 12 Dec. 2023
Revised: 19 Feb. 2024
Accepted: 5 Apr. 2024
Published: June 2024

How to cite:
Chiweshe, T.T., Mokhahlane, L.S., and Welman-Purchase, M. 2024. Kinetic study of reaction formation of phosphate products from thermal dissolution of wolframite using fusion technique. *Journal of the Southern African Institute of Mining and Metallurgy*, vol. 124, no. 6. pp. 339–348

DOI ID:
http://dx.doi.org/10.17159/2411-9717/3215/2024

ORCID:
T.T. Chiweshe
https://orcid.org/0000-0002-9144-164X
L.S. Mokhahlane
https://orcid.org/0000-0001-7833-042X
M. Welman-Purchase
https://orcid.org/0000-0002-7588-2728

Abstract

This study examined an alternative technique of extracting tungsten from wolframite ore using a fusion method with ammonium phosphate salt. Current techniques use alkali salts to decompose tungsten ores and use various purification methods to produce ammonium paratungstate, which is a key intermediate precursor in the extraction of tungsten. In this study, a two-step extraction process, which involves thermal decomposition of the ore using fusion and a separation stage, is examined. The novelty of this technique is the ability to completely decompose wolframite ore and form an unstable tungsten oxide phosphate ($WO_2(PO_3)_2$) compound. The instability of $WO_2(PO_3)_2$ in deionized water enables selective isolation of tungsten as insoluble precipitates of WO_3 and WO_2. The decomposition reaction of $WO_2(PO_3)_2$ is influenced by the presence of oxygen and determined to be first order under ambient conditions. Scanning electron micrographs and X-ray diffraction analysis showed above 80% of the tungsten precipitated compared with the amount that remained in the filtrate solution.

Keywords

tungsten, tungsten oxide phosphate, wolframite ore, fusion extraction, ammonium phosphate flux

Introduction

Tungsten is commonly found in nature in the form of tungstate minerals, which are iron–manganese tungstate (wolframite) and calcium tungstate (scheelite). Wolframite [(Fe, Mn)WO_4] and scheelite ($CaWO_4$) tungstates are the major sources of tungsten that are of economic importance. Tungsten is widely used in various applications due to its excellent thermal and electrical conductivity, high melting point, hardness, and remarkable strength, such as in steel alloys, electrical wires, light bulb filaments, missile components, and armour-piercing projectiles (aerospace and defence industries) (Han et al., 2021). In South Africa, tungsten occurs in the large Riviera deposits situated in Namaqua Metamorphic Complex situated in the Northern Cape Province (Rozendaal et al., 1994). The estimated ore reserve in this area is ~ 46 Mt, with an average grade of at least 0.22% WO_3 (Walker, 1994). China is the major global producer of tungsten, accounting for more than 82%; Vietnam, Russia, Mongolia, Bolivia, Austria, and Rwanda are amongst other top producers.

Tungsten ore is extracted using underground or open-pit mining techniques, depending on the geology and mineralogy of the ore deposits. The ore is usually crushed and ground into fine particles to liberate the tungsten-bearing particles. Beneficiation of the ore is achieved using gravity concentration, magnetic separation, and flotation methods. These processes are sometimes supplemented by other various metallurgical methods, such as leaching, roasting, and magnetic or high-tension separation to obtain clean tungsten concentrate. Leaching and roasting are the most common techniques used in the production of tungsten concentrate. The concentrate is converted to sodium tungstate (Na_2WO_4) solution via alkali digestion (NaOH, Na_2CO_3, etc.) at high temperature (Figure 1). The resultant sodium tungstate solution is then further processed to an intermediate product, ammonium paratungstate (APT), which is a precursor to the pyrometallurgical extraction of pure tungsten metal or carbide (Lassner and Schubert, 1999). Although satisfactory tungsten recovery (above 75 %) has been reported using this technique, the process is cumbersome and generates highly toxic waste products (Olayiwola et al., 2023).

Leaching remains the preferred technique for decomposing/digestion of tungsten ores, despite the high production cost involved in this process, as well as the formation of toxic waste products and other heteropolytungstates, [$(AsW_{12}O_{40})^{3-}$, $(SiW_{12}O_{40})^{4-}$, and $(PW_{12}O_{40})^{3-}$] ions, which contain impurities (Goddard, 1982; Lassner, 1995). Various studies have examined the use of different leaching techniques,

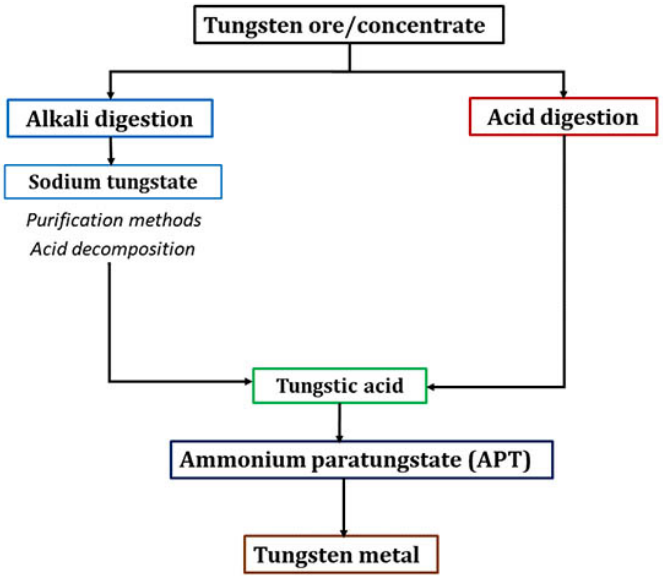

Figure 1—Summary of most-used techniques in tungsten recovery process

such as alkaline pressure leaching (Luo et al., 2021) and leaching by hydrodynamic and acoustic cavitation (Johansson et al., 2021). Research trends show that these leaching techniques work better with scheelite than wolframite (Gong et al., 2019). The decomposition of wolframite using these techniques is reported to be low (30%–50%) compared with scheelite ores or concentrates. However, leaching techniques that involve roasting with alkali salts are still considered better alternatives in decomposing wolframite ore (Srinivas et al., 2000).

A study carried out by Chiweshe (2019) shows a fusion technique using ammonium phosphate flux that was used to liberate tungsten from wolframite ore. Complete sample dissolution was achieved using moderate temperatures (800°C) within minutes (~ 20 min). The most intriguing feature was the formation of tungsten oxide phosphate, ($WO_2(PO_3)_2$), which was found to be unstable in air. The instability of $WO_2(PO_3)_2$ was accompanied by the formation of a precipitate that was presumed to contain tungsten. This two-step dissolution technique was key in further investigating an alternative procedure for the recovery of tungsten from wolframite ore without the formation of APT. This decomposition process prompted a revisit of this study with the aim of determining the rate at which tungsten is formed, chemical composition of the products, and purity of the isolated tungsten products. The objective of this study was to critically determine factors and conditions involved in the quantitative precipitation of tungsten from wolframite ore using this fusion technique.

Experimental

Chemicals, materials, and glassware

Ammonium hydrogen phosphate, $(NH_4)_2HPO_4$ and $NH_4H_2PO_4$ (99%), tungsten(VI) oxide (WO_3) (99%), and orthophosphoric acid (H_3PO_4, 98%) were purchased from Merck Chemicals. The multi-element standard (100 mg/L) was purchased from de Bruyn Spectroscopic Solutions (South Africa). The ceramic crucibles (150 mL) were purchased from Terra Nova Ceramics (South Africa). The quartz cuvettes used for ultraviolet–visible (UV–vis) spectroscopy were supplied by Lasec South Africa. Volumetric flasks were of Blaubrand type grade (A).

Description of wolframite ore

The wolframite ore sample used in this study was obtained from a mine in Namaqualand in the Northern Cape Province of South Africa. The supplied ore was crushed and milled to < 75 µm and supplied in 100 g units. The ore was used in its original state without further purification.

Instrumentation

A Malvern Panalytical Empyrean 4kW X-ray diffractometer (XRD) with Cu-K radiation (~ 0.154 nm) in the 3.5–70° 2θ range and a Rigaku Primus IV wavelength-dispersive X-ray fluorescence (WDXRF) spectrometer were used for elemental analysis of the wolframite ore sample. A Lasec heating furnace (Laboratory and Scientific Equipment Company (Pty) Ltd) was used for sample dissolution. The resultant coloured solutions were analysed using a Varian (Cary 50) UV–vis spectrometer. pH measurements were performed using a Eutech CyberScan (pH 1500) meter. Elemental analysis of the filtrate solutions was performed using a Perkin-Elmer Nexion (model 2000c) inductively coupled plasma mass spectrometer (ICP-MS) using the conditions set out in Table I.

General experimental procedure: Fusion of WO_3 and wolframite ore

Complete sample dissolution of WO_3 and wolframite samples (1.0 g) was achieved using the fusion method described by Chiweshe (2019). The resultant melts were dissolved in deionized water and acetone. Melts dissolved in deionized water formed purple-coloured solutions whilst a purple-coloured residue formed using acetone. The coloured solutions decomposed to form a colourless solution and grey precipitate. The instability of these solutions was determined using UV–vis spectroscopy. The precipitates were collected, dried at room temperature, and analysed using scanning electron microscopy (SEM), X-ray diffraction (XRD), and TESCAN integrated mineral analyzer (TIMA) analysis. The filtrate solution was analysed for elemental content using ICP-MS.

Table I

Selected inductively coupled plasma mass spectrometry operating conditions for elemental analysis using kinetic energy discrimination mode

Parameter/Component	Value/Type/Mode
Nebulizer gas flow	0.96 L/min
Auxiliary gas flow	1.2 L/min
Radio frequency power	1100 W
Plasma gas flow	15 L/min
Rinsing time	60 s
Nebulizer	Meinhard concentric type A3
Spray chamber	Baffled quartz cyclonic
Scanning mode	Peak hopping
Dwell time	50 ms
Replicates	3
Integration time	1 ms
Torch position	X (–1.52 mm), Y (–0.33 mm), Z (0.00 mm)
Mode of operation	Standard mode/kinetic discrimination energy (KED) using helium gas

Scanning electron microscopy- energy-dispersive spectroscopy (SEM-EDS) analysis of WO_3 and wolframite precipitates

SEM-EDS was used for the analysis of the WO_3 and wolframite precipitates. The precipitates were mounted on stubs (Cambridge pin type, 10 mm) using double-sided carbon tape and coated with iridium (± 10 nm) using a Leica EM ACE600 coating system (Austria). Specimens were imaged and analyzed using a JSM-7800F extreme-resolution analytical field-emission SEM (JEOL, Japan).

X-ray diffraction (XRD) analysis of WO_3 and wolframite precipitates

Preliminary investigation was conducted on extraction of the unstable purple compound previously identified as tungsten oxide phosphate ($WO_2(PO_3)_2$) (Loopstra and Boldrini, 1966). This compound was extracted by dissolving the melt in acetone and filtering the mixture. The residue was kept under inert conditions to prevent decomposition. The pure wolframite ore and their precipitates were analysed using a Malvern Panalytical Empyrean XRD diffractometer. The samples were run on zero-background silicon wafers.

TESCAN integrated mineral analysis (TIMA) of WO_3 and wolframite precipitates

TIMA was used to determine mineral phases in the isolated WO_3 and wolframite precipitates. Elemental and phase maps of minerals were evaluated by EDS using a VEGA3 SEM instrument and X64 TESCAN TIMA 2.4.1. software. The beam specifications were 25 kV accelerating
voltage, 43 µA emission current with a working distance of 15.00 mm, a specimen beam current of 17.68 nA, and spot size of 590.00 nm with an absorption current of < 1 pA. The mineral liberation, mineral locking, and mineral association data of minerals of interest were obtained via TIMA software version 2.9.0.

Inductively coupled plasma–mass spectrometry (ICP-MS) analysis of WO_3 and wolframite filtrate solutions

Multi-element calibration standards solutions were prepared in the range of 1.0–500 µg/L using original stock solutions. The solutions were acidified using H_3PO_4 (1.0 mL, 98.0%), including the blank solution, and homogenized before use. Filtrate solutions of WO_3 and wolframite samples were qualitatively analyzed for tungsten content and other major elements (Table II).

Results and discussion

Analysis of fusion of WO_3 and wolframite ore process and comparison of products

Events leading to the precipitation of tungsten were assessed with an objective of establishing the conditions at which tungsten was isolated from wolframite ore. Pure WO_3 was used as a control sample to confirm if the observed chemical changes in wolframite were the result of tungsten. The most notable chemical change (Figure 2(a)) was the formation of tungsten oxide phosphate ($WO_2(PO_3)_2$) in acidic solution, which decomposed in phases to form a precipitate and colourless solution in both samples. The high acidity in both coloured solutions was attributed to the presence of phosphoric acid that formed during the thermal decomposition of ammonium phosphate salt (flux) as shown in Equation [1]:

$$(NH_4)_2H(PO_4) \xleftrightarrow{\Delta\ 800\ °C} H_3PO_4 + 2NH_3\uparrow \quad [1]$$

It is worth mentioning that both melts were soluble in polar solvents and insoluble in organic solvents. Interestingly, dissolution of the melt using acetone enabled $WO_2(PO_3)_2$ to be isolated as a residue. The isolated purple product subsequently decomposed, as shown in Figure 2(b), to form a brown and colourless oily liquid that left a permanent mark that never dried. This oily product was viscous and acidic (pH < 1.5), which further confirmed the instability of $WO_2(PO_3)_2$ in air (oxygen). The stability of $WO_2(PO_3)_2$ was established under inert conditions because no decomposition was observed.

It was evident from the above results that wolframite ore can be successfully converted into solution using ammonium phosphate fusion without requiring any additional digestion/dissolution steps. The novelty of this technique is the ability to convert tungsten into an unstable $WO_2(PO_3)_2$ that decomposed to form an insoluble tungsten species. $WO_2(PO_3)_2$ provided a key step by which tungsten can be selectively isolated from wolframite ore containing a variety of soluble impurities. The rate of decomposition of the purple compound was determined to evaluate the rate at which tungsten precipitated under the prevailing conditions.

Determination of rate of decomposition of $WO_2(PO_3)_2$ in water

The rate of decomposition of $WO_2(PO_3)_2$ was determined using UV–vis spectroscopy. The absorbance spectrum of $WO_2(PO_3)_2$ (Figure 3(a)) showed three peaks with a minor peak at 395 nm, intermediate peak at 640 nm and maximum peak (λ_{max}) at 529 nm.

Table II

Inductively coupled plasma–mass spectrometry analysis comparison of major identified elements in filtrate samples of WO_3 and wolframite ore

Element	WO_3 filtrate (mg/L)	Wolframite filtrate (mg/L)
W	328.4	288.7
Fe	2.11	87.73
Mn	< 1.00	7.24
Al	18.30	23.54

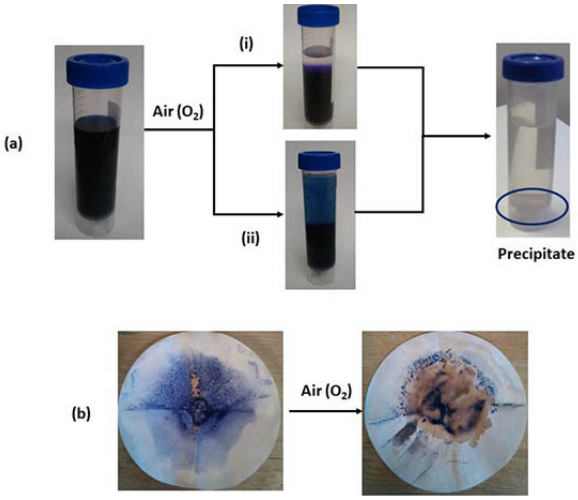

Figure 2—Decomposition reaction of purple $WO_2(PO_3)_2$ solution in (a) water and subsequent decomposition of isolated purple solid product in (b) acetone

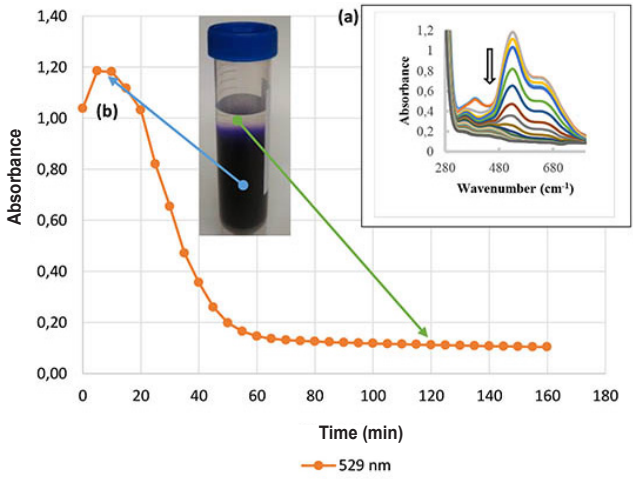

Figure 3—Analysis of colour change of $WO_2(PO_3)_2$ solution using (a) UV–vis absorbance spectra and (b) determination of rate of change of reaction at maximum absorbance (λ_{max}) of 529 nm

Figure 3(b) shows the decomposition of $WO_2(PO_3)_2$ recorded at 5 min intervals. The increase in absorbance recorded in the first 5 min was the result of the colour development that occurred during the dissolution phase. Maximum colour intensity was attained shortly after dissolution, which was preceded by decomposition of $WO_2(PO_3)_2$. The decomposition was influenced by the presence of air (oxygen) and occurred within 1 h.

The rate of decomposition of $WO_2(PO_3)_2$ was studied by probing the rate of change in colour of the purple solution ($WO_2(PO_3)_2$) to colourless with time at room temperature, as shown in Figure 3(b). The purple colour change of the solution followed a first-order rate law, which can be expressed by Equation [2], where $A(t)$ is the concentration of $WO_2(PO_3)_2$ at time (t), $A(0)$ is the initial concentration at time (t_0), and λ is the first-order rate constant:

$$A(t) = A(0)\exp(-\lambda t) \quad [2]$$

The half-life ($t_{1/2}$) of $WO_2(PO_3)_2$ is represented by Equation [3]:

$$A(t) = \frac{A(0)}{2} \quad [3]$$

Equations [2] and [3] can be simplified to give the rate of the reaction (Equation [6]):

$$\frac{A(0)}{2} = A(0)\exp(-\lambda t_0) \quad [4]$$

$$\frac{1}{2} = \exp(-\lambda t_0) \quad [5]$$

$$-In2 = -\lambda t_0 \quad [6]$$

$$\lambda = \frac{\ln 2}{t_0} \quad [7]$$

The time taken (t for the complete colour change was 60 min. It was therefore presumed that the rate of decomposition of the purple $WO_2(PO_3)_2$ was 0.012 min^{-1}.

Proposed mechanism

The formation and decomposition of $WO_2(PO_3)_2$ are postulated to occur according to Equations [8] and [9], respectively:

$$WO_3(s) + 2(NH_4)_2HPO_4(s) \xrightarrow{800^oC} WO_2(PO_3)_2(s) + HN_3(g) + H_2O(g); \quad [8]$$

$$WO_2(PO_3)_2(s) + H_2O(l) \xrightarrow{O_2} W_xO_y(s) + 2H_2PO_3^-(aq) + H^+, \quad [9]$$

where W_xO_y = WO_2, WO_3, or $W_{25}O_{73}$)

The increase in acidity, as determined from the residue following decomposition of $WO_2(PO_3)_2$, is postulated to result from the formation of orthophosphoric acid (H_2PO_3). The formation of H_2PO_3 shown Equations [1] and [8] accounts for the high acidity (pH < 1.5) of the remaining solution. The variation in the formation of tungsten products was caused by inconsistent decomposition of the $WO_2(PO_3)_2$, as shown in Figure 3(a).

Characterization of isolated tungsten products

Scanning electron microscopy analysis

SEM images in Figure 4 show micro-crystalline particles of the precipitates from (a) WO_3 and (b) wolframite ore analysed at 10 000 μm magnification and spatial resolution of 1 μm. Figure 6 compares the XRD pattern of the precipitates with the corresponding patterns from the ICDD-PDF 2 2021 database. The crystalline particles appeared clustered and isometric (A) whilst some (lower quantity) appeared to be tetragonal in shape (B). SEM images identified the presence of two particles (A and B) in both precipitates with similar faceted morphology. This similarity in morphology suggests the same chemical composition. The occurrence of two different particles (isometric and tetragonal) in both precipitates indicated the presence of more than one product. The EDS analysis in Table III shows elemental estimates of tungsten and impurities in both precipitates. Details of these two different compounds will be included in future studies.

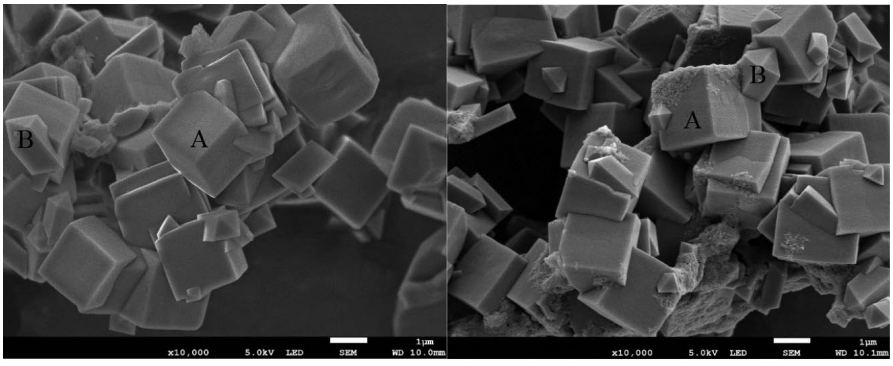

Figure 4—Scanning electron micrographs showing similarity of particles A (isometric) and B (tetragonal) in both precipitates. (Left) WO_3 and (right) wolframite ore

Table III

Energy-dispersive spectroscopy elemental composition of precipitates obtained from WO_3 and wolframite ore

Element	Line type	WO_3 precipitate (mass%)	Wolframite ore precipitate (mass%)
O	K series	16.74	16.29
Mn	K series	< 1	1.45
Fe	K series	5	22.62
W	**M series**	**60.29**	**59.47**
Na	K series	< 1	< 1
P	K series	< 1	< 1
S	K series	< 1	< 1

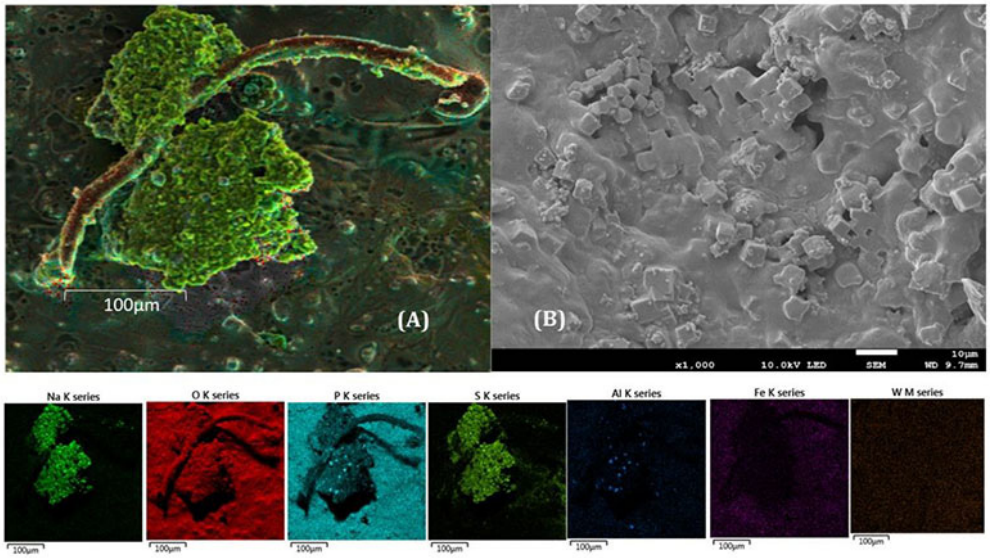

Figure 5—Scanning electron microscopy energy-dispersive spectroscopy showing (A) elemental mapping of solid precipitate ($WO^2(PO_3)_2$) and (B) the crystalline particles isolated using acetone

Figure 5 shows micrographs and inserts of the mapping images from the solid product isolated using acetone. The precipitate appeared molten, with visible cubic crystalline particles embedded in the product. The crystal morphology of the particles in this isolated product was the same as in the precipitate; however, the molten state of this product contained impurities that revealed differences in the elemental composition between the precipitate and the isolated solid product. Most elements identified in this molten state were soluble in water and were not present in the precipitate after the decomposition of $WO_2(PO_3)_2$.

X-ray diffraction analysis

Analysis of the precipitates by powder XRD was mainly conducted for phase identification and sample purity. The diffractograms displayed in Figure 6 revealed that the wolframite sample consisted of wolframite, quartz, and elsmoreite. This diffractogram had no similarity to that of the WO_3 sample, which was a purchased laboratory-grade chemical. Although these differences were prominent, the profoundness of the similarity in the precipitation products, post fusion, is quite evident. This similarity suggests the presence of similar compounds within the precipitates. The ICDD 01-071-2141 (Loopstra and Boldrini, 1966) of WO_3 was referenced as the monoclinic structured variant. Similar compounds corresponding to WO_2 (ICDD 01-071-0614) (Palmer and Dickens, 1979) and $W_{25}O_{73}$ (ICDD 01-071-0070) (Sundberg, 1976) were detected. Peaks corresponding to $WOPO_4$ (ICDD 00-044-0349) (Kinomura et al., 1988) were also found, which presumably were a remnant of $WO_2(PO_3)_2$.

TESCAN integrated mineral analysis

The elemental distributions of the wolframite ore sample and isolated precipitates are given in Table IV. All information pertaining to tungsten(VI) oxide (WO_3) (99%) was obtained from the supplier and this chemical was not subjected to initial characterization chemical analysis. Tungsten was present in all samples, as expected, with the wolframite recording the highest tungsten content at 47.57 vol.% from the TIMA analysis (Table IV). This is the amount of tungsten in the sample as-received from the mine before any fusion process took place. XRF analyses were utilized to supplement the TIMA analyses: high levels of tungsten were also recorded for the wolframite ore, at 75.8 mass%. A sharp drop in tungsten was observed in the precipitate that formed after the wolframite underwent fusion, with 0.12 vol.% tungsten recorded (i.e., wolframite precipitate) for TIMA analysis. XRF was used to supplement the TIMA analysis and recorded 23.1 mass% tungsten for the wolframite precipitate. These two analytical

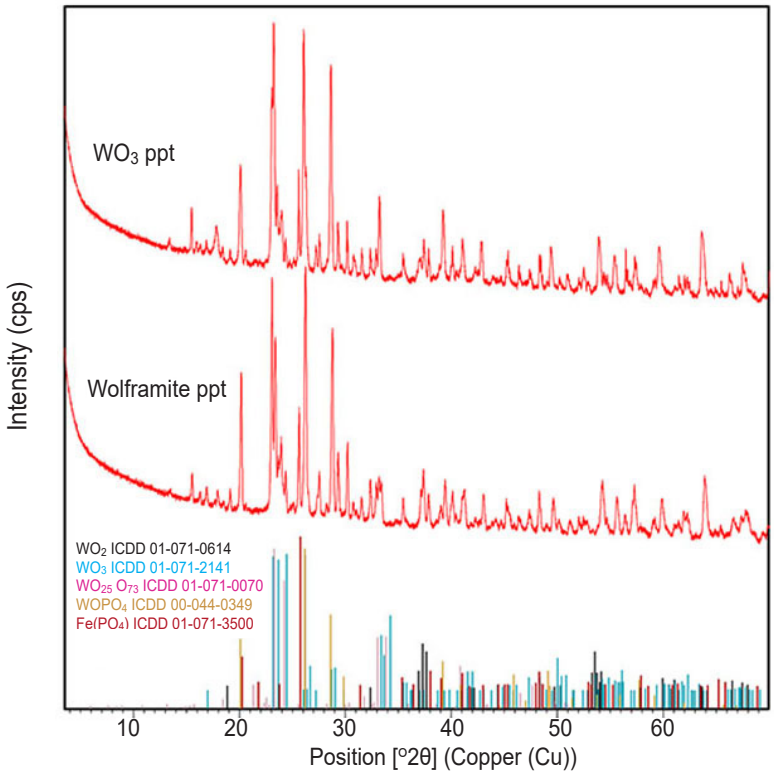

Figure 6—Diffractograms of original wolframite and WO_3 precipitates (ppt)

techniques showed a sharp decrease in tungsten concentration in the precipitate, which means that the material that precipitated out of solution after the fusion process will likely have lower levels of tungsten and some tungsten will remain in solution. The tungsten(VI) oxide (WO_3) (99%) from Merck Chemicals was used as a blank to ascertain the effectiveness of the fusion for a known tungsten-enriched substance (i.e., 99% WO_3). Interestingly, the amounts of tungsten recorded after the fusion process from both the WO_3 and wolframite precipitates were exactly 0.12 vol.%. This means that the fusion process was effective to almost the same extent and the final precipitates were similar, as seen in the XRD results, regardless of the starting material. The two precipitates contained zirconium, yttrium, silicon, and phosphorus as major elements (Table IV). Phosphorus was introduced by the flux as part of the fusion products. Zirconium and yttrium were likely introduced from the fusion process; for example, oxide refractories such as ZrO_2 are normally used as crucible materials due to their excellent thermal properties, but are reported to react and dissolve into the melt during fusion (Song et al., 2022).

The primary phases contained in the samples are displayed in Table V. The wolframite ore recorded the highest wolframite content at 78.5 vol.%. There was a very small volume of wolframite observed in the wolframite precipitate, recording only 0.19 vol.%. This shows that little or no wolframite can be expected to precipitate from solution after the fusion process. However, tungsten and phosphorus compounds were determined in the precipitates from XRD results. The WO_3 precipitate also recorded a wolframite concentration of 0.19 vol.%. The XRD results had two very distinct and similar patterns for the two precipitates, although the starting materials were different (i.e., laboratory-grade tungsten oxide and wolframite ore from the mine); however, XRD detected a variety of other tungsten derivative phases that may not be defined within the TIMA analysis spectrum. The major phases that precipitated from solution were zircon and xenotime–yttrium, as seen in Table V. These elements were not present in the original materials, so could have been incorporated into the fusion process from the crucible material.

A backscattered-electron image of the wolframite ore is presented in Figure 7 (top). The scan shows that this ore was highly enriched in wolframite (almost all dominant purple colour), with small grains of quartz also present. The two precipitate scans were similar, with zircon grains that mostly had an elongated oval shape and xenotime–yttrium grains generally associated/centred around the zircon. Wolframite was minor compared with the dominant zircon and xenotime–yttrium minerals and its distribution was not associated with any grains or pattern for the two precipitates, as displayed in Figure 7 (middle and bottom). This suggests that the precipitates were composed of almost new products, regardless of the starting material, and the phases that precipitated were more associated with the elements detected from the interaction with the crucible rather than the ore itself.

Comparing the XRD and TIMA results revealed consistency of the starting materials. A large portion of the TIMA results were unclassified: these are believed to be the W–P–O compounds that are expressed in the XRD results. This corresponds with the XRF results, which also detected Fe, W, and P.

Inductively coupled plasma–mass spectrometry analysis

The filtrate solution that remained after isolation of the precipitate was analysed to determine the composition of the remaining elements in solution. The pH values of both filtrate solutions (pH 1.2–1.6) were adjusted to pH 4.5–5.5 prior to analysis. The acid matrix of the calibration standards was matched with those of the samples. The KED analysis technique was used for quantitative

Table IV
TESCAN integrated mineral analysis showing elemental distribution in each sample

Element	Wolframite ore (vol.%)	Wolframite precipitate (vol.%)	WO_3 precipitate (vol.%)
Tungsten	47.57	0.12	0.12
Oxygen	17.04	9.15	12.28
Zirconium	0.00	8.30	10.55
Silicon	0.42	2.96	4.53
Iron	7.23	0.02	0.03
Manganese	7.11	0.02	0.02
Yttrium	0.00	3.35	2.95
Phosphorus	0.00	2.65	2.33
Hafnium	0.00	0.90	1.14
Ytterbium	0.00	0.92	0.81
Dysprosium	0.00	0.91	0.80
Erbium	0.00	0.77	0.68
Gadolinium	0.00	0.44	0.39
Aluminium	0.00	0.05	0.56
Samarium	0.00	0.14	0.12

Table V
Primary phases detected in samples from TESCAN integrated mineral analysis

Primary phase	Wolframite precipitate (vol.%)	WO_3 precipitate (vol.%)	Wolframite ore (vol.%)
Wolframite	0.19	0.19	78.45
Zircon	19.20	24.38	0.00
Xenotime-(Y)	11.60	10.20	0.00
Kaolinite	0.21	2.62	0.00
Quartz	0.18	0.75	0.89
Tantalite-(Fe)	0.03	0.02	0.04
Baddeleyite	0.03	0.05	0.00
Beryl	0.01	0.03	0.00
Tantalite-(Mn)	0.02	0.01	0.00
Cuprite	0.01	0.00	0.00
Scheelite	0.00	0.00	0.01
Total	31.50	38.30	79.41

analysis due to its ability to minimize interferences caused by polyatomic ions. The filtrate solution of WO_3 showed the presence of W (328 mg/L), and trace amounts of Fe (2 mg/L) and Al (18 mg/L). The filtrate solutions of wolframite ore showed the presence of four major elements: W (289 mg/L), Fe (88 mg/L), Al (24 mg/L), and Mn (7 mg/L). The source of tungsten in solution is presumed to be from incomplete decomposition of the purple $WO_2(PO_3)_2$ compound. Although a larger proportion of the tungsten was reported in the precipitate, the precipitation of tungsten was largely influenced by the decomposition reaction.

Conclusion

The use of the ammonium phosphate fusion method was shown to be a promising technique in the extraction of tungsten from wolframite ores. The key beneficial factor in this technique is the formation of $WO_2(PO_3)_2$, which decomposed to form various insoluble tungsten species of WO_3 and WO_2 under ambient conditions; however, both WO_3 and wolframite ore revealed similar tungsten concentrations in the filtrate solutions. This was presumed to be the result of incomplete decomposition of $WO_2(PO_3)_2$ and needs further investigation.

Acknowledgements

The author would like to thank the Research Fund of the University of the Free State, South Africa, for financial support.

Credit author statement

TTC: Conceptualization - formulation or evolution of overarching research goals and aims, Methodology - Development or design of methodology, Writing - Original draft preparation, Investigation -

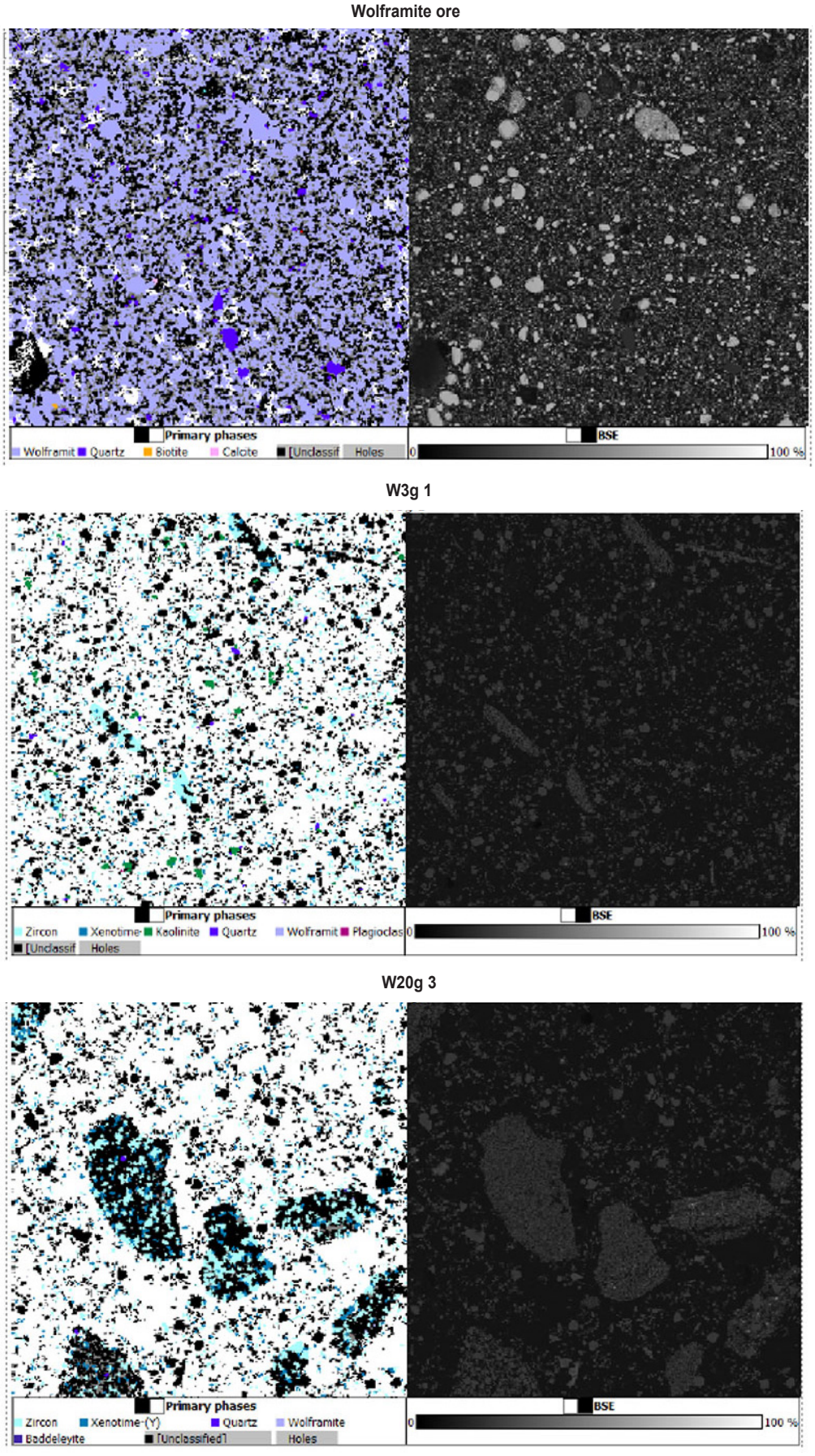

Figure 7—TESCAN integrated mineral analysis, showing primary mineral phases in wolframite ore (top), WO_3 precipitate (middle), and wolframite precipitate (bottom)

Laboratory analysis and interpretation
LSM: Investigation - Laboratory analysis and interpretation, Writing - Original draft preparation, Writing - Reviewing and Editing.
MWP: Investigation - Laboratory analysis and interpretation, Writing - Original draft preparation.

Conflict of interest

The authors declare that they have no conflict of interest.

References

Chiweshe, T.T. 2019. Characterization of molybdenum and tungsten phosphates compounds prepared using ammonium phosphate salt as flux. *Bulletin of the Chemical Society of Ethiopia*, vol. 33, no. 1, pp. 103–112.

Goddard, J.B. 1982. Purification of ammonium tungstate solutions. US Patent No. 4,346, 061, Aug. 24.

Gong, D., Zhou, K., Peng, C., Li, J., and Chen, W. 2019. Sequential extraction of tungsten from scheelite through roasting and alkaline leaching. *Minerals Engineering*, vol. 132, pp. 238–244.

Han, Z., Golev, A., and Edraki, M. 2021. A review of tungsten resources and potential extraction from mine waste. *Minerals*, vol. 11, p. 701.

Johansson, Ö., Pamidi, T., and Shankar, V. 2021. Extraction of tungsten from scheelite using hydrodynamic and acoustic cavitation. *Ultrasonics Sonochemistry*, vol. 71, pp. 105408.

Kinomura, N., Hirose, M., Kumada, N., Muto, F., and Ashida, T. 1988. Preparation of a new tungsten(V) phosphate and its polymorph. *Journal of Solid State Chemistry*, vol. 77, pp. 156 –161.

Lassner, E. 1995. From tungsten concentrates and scrap to highly pure ammonium paratungstate (APT). *International Journal of Refractory Metals and Hard Materials*, vol. 13, no. 1, pp. 35–44.

Lassner, E. and Schubert, W.-D. 1999. Industrial production. In *Tungsten*, Lassner, E. and Schubert, W.-D. (eds.), Springer, Boston.

Loopstra, B.O. and Boldrini, P. 1966. Neutron diffraction investigation of WO_3. *Acta Crystallographica*, vol. 21, no. 1, pp. 158–162.

Luo, Y., Chen, X., Zhao, Z., Liu, X., Li, J., He, L., and Sun, F. 2021. Pressure leaching of wolframite using a sulfuric-phosphoric acid mixture. *Minerals Engineering*, vol. 169, pp. 106941.

Olayiwola, A.U., Du, H., Wang, S.-N., Liu, B., Lv, Y.-Q., and Pan, B. 2023. Cleaner production of ammonium paratungstate by membrane electrolysis-precipitation of sodium tungstate solution. *Tungsten*, vol. 5, no. 1, pp. 145–159.

Palmer, D.J. and Dickens, P.G. 1979. Tungsten dioxide: structure refinement by powder neutron diffraction. *Acta Crystallographica Section B*, vol. 35, no. 9, pp. 2199–2201.

Rozendaal, A., Gresse, P.G., Scheepers, R., and de Beer, C.H. 1994. Structural setting of the Riviera W-Mo deposit, western Cape, South Africa. *South African Journal of Geology*, vol. 97, no. 2, pp. 184–195.

Song, Q., Liang, T., Qian, K., Xing, W., Zha, X., Chen, B., Ma, Y., and Liu, K. 2022. Corrosion resistance of calcium zirconate crucible to titanium-copper melts. *Journal of the European Ceramic Society*, vol. 42, no. 7, pp. 3321–3331.

Sundberg, M.R. 1976. The crystal and defect structures of $W_{25}O_{73}$, a member of the homologous series W_nO_{3n-2}. *Acta Crystallographica Section B: Structural Crystallography and Crystallographic Chemistry*, vol. 32, pp. 2144–2149.

Srinivas, K., Sreenivas, T., Natarajan, R., and Padmanabhan, N.P.H. 2000. Studies on the recovery of tungsten from a composite wolframite–scheelite concentrate. *Hydrometallurgy*, vol. 58, no. 1, pp. 43–50.

Walker, P.W.A. 1994. Riviera tungsten - a discovery case history. *Exploration Mining Geology*, vol. 3, pp. 349–356. ◆